Nuclear Engineering and Technology 49 (2017) 1143–1156

Contents lists available at ScienceDirect

Nuclear Engineering and Technology

journal homepage: www.elsevier.com/locate/net

Original Article

Recent developments in the GENESIS code based on the Legendre polynomial expansion of angular flux method

Akio Yamamoto*, Akinori Giho, Tomohiro Endo

Nagoya University, Furo-cho, Chikusa-ku, Nagoya 464-8603, Japan

ARTICLE INFO

Article history:
Received 28 May 2017
Received in revised form
26 June 2017
Accepted 27 June 2017
Available online 18 July 2017

Keywords:
Acceleration
Anisotropic scattering
C5G7 Benchmark Problem
GENESIS
Simplified Pn
Stability

ABSTRACT

This paper describes recent development activities of the GENESIS code, which is a transport code for heterogeneous three-dimensional geometry, focusing on applications to reactor core analysis. For the treatment of anisotropic scattering, the concept of the simplified Pn method is introduced in order to reduce storage of flux moments. The accuracy of the present method is verified through a benchmark problem. Next, the iteration stability of the GENESIS code for the highly voided condition, which would appear in a severe accident (e.g., design extension) conditions, is discussed. The efficiencies of the coarse mesh finite difference and generalized coarse mesh rebalance acceleration methods are verified with various stabilization techniques. Use of the effective diffusion coefficient and the artificial grid diffusion coefficients are found to be effective to stabilize the acceleration calculation in highly voided conditions.

1. Introduction

Significant efforts have been devoted to high fidelity simulation methods of core characteristics. Monte Carlo and deterministic methods are two important approaches for high fidelity simulations. As for deterministic methods, spatial, angular, energetic, and temporal resolutions are being continuously increased and three-dimensional (3D) multigroup transport calculations considering explicit 3D heterogeneous geometries of reactor core are becoming feasible (e.g., [1–11]).

Various approaches can be considered for a 3D multigroup transport calculation with explicit heterogeneous geometry. A straightforward approach to realize this type of calculation is the direct application of method of characteristics (MOC) in 3D geometry [9–11]. However, this requires large computational resources (both memory and computation time), and thus its practical application to large-scale geometry, e.g., a commercial light water reactor (LWR), would be limited. Instead, the planar MOC method is successfully applied for high-fidelity core analyses [2–8].

In the planar MOC method, neutron transport calculations for radial and axial directions are performed by the conventional MOC and diffusion/low order transport calculations, respectively. In typical commercial reactors, axial heterogeneity is much smaller than it is in the radial direction, and thus different treatments of neutron transport for radial and axial directions are justified and can be applied without significant loss of prediction accuracy. The planar MOC has a significant advantage in computational efficiency because it uses the conventional MOC in two-dimensional (2D) geometry.

Recently, high fidelity simulations of core characteristics under severe core conditions, e.g., loss-of-coolant accident or anticipated transient without scram, are being required from the viewpoint of safety analysis. In these conditions, the highly voided condition should be considered with significantly skewed power distribution not only for the radial direction but also for the axial direction. Because the planar MOC uses a diffusion or low-order transport method to approximately consider the axial leakage, it would incur degradation of the prediction accuracy and/or convergent issues in severe core conditions. This issue is discussed in detail by Hursin, and some improvements for axial coupling among axial planes are proposed [8].

In order to address this issue, the Legendre polynomial Expansion of Angular Flux (LEAF) method is proposed as an extension of the axially simplified method of characteristics in 3D (ASMOC3D) method [12–14]. In the LEAF method, axial leakage is explicitly considered without approximation. Thus, higher accuracy is

* Corresponding author.
E-mail address: a-yamamoto@nucl.nagoya-u.ac.jp (A. Yamamoto).

http://dx.doi.org/10.1016/j.net.2017.06.016

expected in severe core conditions, including highly voided conditions.

The GENESIS code, based on the LEAF method, is being developed at Nagoya University. The GENESIS code is a multigroup transport code for 2D and 3D heterogeneous geometries. The LEAF method and the conventional MOC are used for 3D and 2D transport calculations, respectively. The GENESIS code can handle various complicated geometries through the factorial geometry method and the R-function solid modeler in rectangular and hexagonal geometries [15,16]. Nested geometry can be allowed at any depth. Thus, very complicated geometry can be treated. The direct neutron path linking technique is used to reduce the computational burden of ray trace in a large and repeated geometry such as those of large power reactors [17]. Higher-order anisotropic scattering with various levels of symmetry (30°, 45°, 60°, 90°, 120°, 180°, both reflective and rotational) can be treated. The two-level generalized coarse mesh rebalance (GCMR) or coarse mesh finite difference (CMFD) method is used as an efficient acceleration method [18,19].

In the present paper, recent developments of the GENESIS code are described.

In Section 2, the fundamental theories of the LEAF method are briefly described. Then, in Section 3, recent developments of the GENESIS code are described. We especially focus on treatment of anisotropic scattering using the concept of simplified Pn (SPn) method, and numerical stability of the GCMR and the CMFD acceleration methods for highly voided condition, which appears under design extension condition in LWRs. Finally, concluding remarks are provided in Section 4.

2. LEAF method

A detailed description of the LEAF method can be found elsewhere [13,14], but a brief description is provided for readers' understanding.

The concept of the LEAF method is shown in Fig. 1. In the conventional "direct" 3D approach of MOC, a 3D geometry is covered by one-dimensional (1D) ray traces, which usually require excessive memory storage for large cores such as those of commercial reactors. In the LEAF method, a geometry is instead covered by planes that are considered extensions of ray traces drawn in 2D x–y geometry to the z direction. A 3D geometry is covered by sets of parallel planes (characteristics planes) for various azimuthal directions. Because extruded geometry for axial direction is considered, we can assume that a characteristics plane is composed of rectangles, as shown in Fig. 1. In the case of MOC, neutron transport calculation on a characteristics line, i.e., in 1D geometry, is carried out. Instead, in the LEAF method, a neutron transport calculation within the characteristics plane, i.e., in 2D geometry, is carried out. Although any neutron transport method can be used for transport calculation within a 2D characteristics plane, the angular-dependent transmission probability (ADTP) method, because of its efficiency, is used in the GENESIS code [20].

In order to reduce spatial discretization error, spatial distributions of incoming and outgoing angular fluxes along faces of a rectangle in a characteristics plane are expanded to second Legendre polynomials. Similarly, the spatial distribution of the neutron source in a rectangle is expanded into first and second orders in radial and axial directions, respectively. It should be noted that angular distribution is treated as a discretized quadrature set.

With the above spatial expansion, outgoing angular fluxes from a rectangle are calculated by:

$$\begin{aligned}\varphi_i^{out,Right} = &\sum_{j=0}^{2}\left(\varphi_j^{in,Left}T_{j,i}(l\to r) + \varphi_j^{in,Bottom}T_{j,i}(b\to r)\right)\\ &+q_0E_{s,0,i}(q\to r) + q_{s,1}E_{s,1,i}(q\to r)\\ &+q_{z,1}E_{z,1,i}(q\to r) + q_{z,2}E_{z,2,i}(q\to r),\end{aligned} \tag{1}$$

$$\begin{aligned}\varphi_i^{out,Top} = &\sum_{j=0}^{2}\left(\varphi_j^{in,Left}T_{j,i}(l\to t) + \varphi_j^{in,Bottom}T_{j,i}(b\to t)\right)\\ &+q_0E_{s,0,i}(q\to t) + q_{s,1}E_{s,1,i}(q\to t)\\ &+q_{z,1}E_{z,1,i}(q\to t) + q_{z,2}E_{z,2,i}(q\to t),\end{aligned} \tag{2}$$

where $\varphi_i^{out,Right}$, $\varphi_i^{out,Top}$, $\varphi_j^{in,Left}$, $\varphi_j^{in,Bottom}$ are the ith or jth spatial expansion coefficients of the outgoing and incoming angular flux spatial distributions, q_0, $q_{s,1}$, $q_{z,1}$, $q_{z,2}$, are expansion coefficients of neutron source spatial distribution, and:

$T_{j,i}(l\to r)$: angular-dependent transmission kernel from jth coefficient of angular flux on the left face to ith coefficient of angular flux on the right face

$T_{j,i}(b\to r)$: angular-dependent transmission kernel from jth coefficient of angular flux on the bottom face to ith coefficient of angular flux on the right face

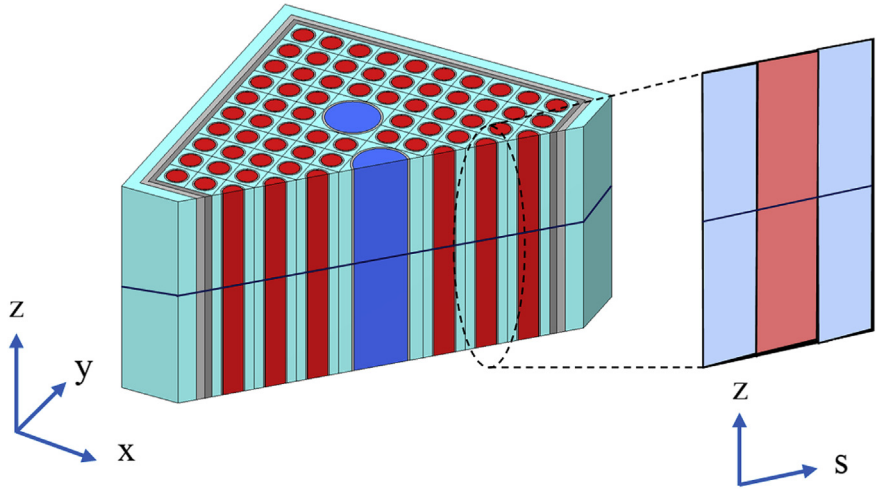

Fig. 1. Concept of the LEAF method. LEAF, Legendre polynomial Expansion of Angular Flux.

$E_{s,k,i}(q\to r)$: angular-dependent escape kernel from kth coefficient of neutron source for radial direction to ith coefficient of angular flux on the right face
$E_{z,k,i}(q\to r)$: angular-dependent escape kernel from kth coefficient of neutron source for z direction to ith coefficient of angular flux on the right face

Note that spatial distributions of incoming and outgoing neutron angular fluxes along faces are expanded as:

$$\psi(s)=\sum_{i=0}^{2}\varphi_i P_i(s),\qquad \psi(z)=\sum_{i=0}^{2}\varphi_i P_i(z), \tag{3}$$

where $P_i(s)$ and $P_i(z)$ are Legendre polynomials of ith order, and s and z are coordinates along horizontal and vertical faces of a rectangle that are normalized from −1 to 1 in a rectangle, respectively.

Then, the transmission and escape probabilities are explicitly calculated by:

$$T_{j,i}(l\to r)=\frac{\int_{-1}^{+1}\psi_{j,l}(z)\cdot P_i(z)dz}{\int_{-1}^{+1}P_i^2(z)dz}, \tag{4}$$

$$T_{j,i}(b\to r)=\frac{\int_{-1}^{+1}\psi_{j,b}(z)\cdot P_i(z)dz}{\int_{-1}^{+1}P_i^2(z)dz}, \tag{5}$$

$$E_{s,k,i}(q\to r)=\frac{\int_{-1}^{+1}\psi_{k,q,s}(z)\cdot P_i(z)dz}{\int_{-1}^{+1}P_i^2(z)dz}, \tag{6}$$

$$E_{z,k,i}(q\to r)=\frac{\int_{-1}^{+1}\psi_{k,q,z}(z)\cdot P_i(z)dz}{\int_{-1}^{+1}P_i^2(z)dz}, \tag{7}$$

where

$\psi_{j,l}(z)$: outgoing angular flux distribution at the right face (along z axis) when incoming angular flux from the left (l) face is given as $P_j(z)$, and other incoming angular fluxes and neutron source are set to zero
$\psi_{j,b}(z)$: outgoing angular flux distribution at the right face (along z axis) when incoming angular flux from the bottom (b) face is given as $P_j(s)$, and other incoming angular fluxes and neutron source are set to zero
$\psi_{k,q,s}(z)$: outgoing angular flux distribution at the right face (along z axis) when neutron source is given as $P_k(s)$, and all incoming angular fluxes are set to zero
$\psi_{k,q,z}(z)$: outgoing angular flux distribution at the right face (along z axis) when neutron source is given as $P_k(z)$, and all incoming angular fluxes are set to zero

A similar expression is used for Eq. (2).
The average angular flux in a rectangle is calculated by:

$$\begin{aligned}\overline{\psi}=&\sum_{j=0}^{2}\left(\varphi_j^{in,Left}C_j(l\to a)+\varphi_j^{in,Bottom}C_j(b\to a)\right)\\&+q_0C_{s,0}(q\to a)+q_{s,1}C_{s,1}(q\to a)\\&+q_{z,1}C_{z,1}(q\to a)+q_{z,2}C_{z,2}(q\to a),\end{aligned} \tag{8}$$

where

$C_j(l\to a)$: angular-dependent collision kernel from jth coefficient of angular flux on the left face to average angular flux in the rectangular region
$C_j(b\to a)$: angular-dependent collision kernel from jth coefficient of angular flux on the bottom face to average angular flux in the rectangular region
$C_{s,k}(q\to a)$: angular-dependent collision kernel from kth coefficient of neutron source for radial direction to average angular flux in the rectangular region
$C_{z,k}(q\to a)$: angular-dependent collision kernel from kth coefficient of neutron source for z direction to average angular flux in the rectangular region

The collision kernel is explicitly calculated by:

$$C_j(l\to a)=\int_{-1}^{+1}\int_{-1}^{+1}\psi_{j,l}(s,z)dzds, \tag{9}$$

$$C_j(b\to a)=\int_{-1}^{+1}\int_{-1}^{+1}\psi_{j,b}(s,z)dzds, \tag{10}$$

$$C_{s,k}(q\to a)=\int_{-1}^{+1}\int_{-1}^{+1}\psi_{k,q,s}(s,z)dzds, \tag{11}$$

$$C_{z,k}(q\to a)=\int_{-1}^{+1}\int_{-1}^{+1}\psi_{k,q,z}(s,z)dzds, \tag{12}$$

where

$\psi_{j,l}(s,z)$: angular flux distribution at (s,z) in a rectangle when incoming angular flux from the left (l) face is given as $P_j(z)$, and other incoming angular fluxes and neutron source are set to zero
$\psi_{j,b}(s,z)$: angular flux distribution at (s,z) in a rectangle when incoming angular flux from the bottom (b) face is given as $P_j(s)$, and other incoming angular fluxes and neutron source are set to zero
$\psi_{k,q,s}(s,z)$: angular flux distribution at (s,z) in a rectangle when neutron source is given as $P_k(s)$, and all incoming angular fluxes are set to zero
$\psi_{k,q,z}(s,z)$: angular flux distribution at (s,z) in a rectangle when neutron source is given as $P_k(z)$, and all incoming angular fluxes are set to zero

Because we already know the incoming and outgoing angular fluxes, the average angular flux in a rectangular region can be calculated using the neutron balance equation and a neutron source. However, in a highly voided region, the total cross section will be very small, and magnitudes of incoming and outgoing angular fluxes will be similar. Thus, in the neutron balance calculation, large comparative values are canceled out (outgoing angular flux is subtracted from incoming angular flux), which would result in significant round off error. Furthermore, the subtracted result is

divided by a small total cross section. This is a typical situation that can cause numerical instability, and thus Eq. (8) is used instead in the GENESIS code.

Once average angular flux in a rectangle is obtained, the average scalar flux in a flux region can be obtained through integration in phase space (spatial and angular domain), which is essentially the same procedure used in the conventional MOC method.

$$\overline{\phi} = \frac{1}{V}\int \psi dV d\Omega \approx \frac{\sum_m \omega_m \sum_k \delta A_{m,k} \Delta s_{m,k} \Delta z \overline{\psi}_{m,k}}{\sum_m \omega_m \sum_k \delta A_{m,k} \Delta s_{m,k} \Delta z} \tag{13}$$

where

$\overline{\phi}$: average scalar flux in a flux region in 3D geometry
ω_m: weight of a solid angle quadrature set for direction m
$\delta A_{m,k}$: ray trace width for direction m, ray trace k
$\Delta s_{m,k}$: face length of a rectangular region in a characteristics plane for radial direction (direction m, ray trace k), which corresponds to the segment length of ray trace in the conventional 2D MOC
Δz: face length of a rectangular region in a characteristics plane for axial direction
$\overline{\psi}_{m,k}$: average angular flux in a rectangular region obtained by Eq. (8) (direction m, ray trace k)

In the LEAF method, spatial distribution of scalar flux is considered in order to reduce spatial discretization error. Distributions up to the first (linear) and second (quadratic) spatial moments are considered for radial and axial directions, respectively. In the radial direction, the weighted residual method is used to estimate spatial moments [21]. In the axial direction, average scalar fluxes at the top and bottom mesh surfaces, and average scalar flux in the mesh, are used to fit a quadratic scalar flux distribution. The spatial distributions of scalar flux for radial and axial directions are used to evaluate expansion coefficients of spatial neutron source distribution, which appear in Eqs. (1), (2), and (8).

As shown in Eqs. (1), (2), and (8), the transmission, escape, and collision kernels are used in the LEAF method. These kernels are very frequently evaluated; they correspond to the exponential function that appeared in the conventional MOC in 2D geometry. Therefore, their evaluation speed dominates total execution time in actual implementation. In principle, their evaluation can be easily performed by numerical integration using ray traces in the rectangle region appearing in the LEAF calculation. A straightforward approach to estimate these kernels is on-the-fly estimation using numerical integrations with ray traces. However, such an approach is equivalent to the direct 3D MOC method, which requires longer computation time. Thus, in the GENESIS code, transmission, escape, and collision kernels are evaluated and tabulated prior to transport sweeps.

The kernels depend on the mesh sizes for radial and axial directions, total cross section, and polar direction. In actual reactor analysis applications, mesh sizes of axial direction can be classified into several types, e.g., core and reflector parts. Similarly, polar directions are discretized into several angles. Therefore, in the GENESIS code, axial mesh size and polar direction are explicitly treated (i.e., not considered as interpolation parameters and tabulated in different tables). For the kernels, only radial mesh size and total cross section are used as interpolation parameters in the pretabulated table. Significant reduction in computation time can be achieved by using the tabulation method. However, in the execution time of the GENESIS code, interpolation of the kernels still takes a major part.

Number of floating point operations required per rectangle (mesh) and angle in the LEAF method depends on the order of spatial expansions for scalar flux in a rectangle and incoming/outgoing angular fluxes at faces. As a typical situation, when first-order expansion is applied to scalar flux and angular fluxes, required floating point operations would be approximately 60 per rectangle and angle. A conventional MOC sweep with linear source approximation requires approximately 10 floating point operations and two 1D table interpolations, which means approximately 15 floating point operations are necessary per segment and angle. When number of ray traces in a mesh is precomputed in 3D MOC and if four ray traces are used to cover a mesh for axial direction, required numbers of floating point operations are comparable between the LEAF method and the conventional 3D MOC. However, when the mesh size for radial direction (a few centimeters) is considered, 3D MOC requires a larger number of floating point operations even if on the fly ray tracing is not carried out. In any case, the table interpolation is a dominant part of the computational load in the LEAF method, and its efficient computation is an open problem.

In the present study, interpolation axes for radial mesh size and total cross section are determined by preliminary sensitivity calculations and given by input data. The automated setting of interpolation axes will be useful and is an important task in future. Note that memory storage required for interpolation tables is small. Their typical total size is on the order of a few megabytes (MB).

The GENESIS code adopts rigorous treatment at the reflective boundary for radial directions, i.e., outgoing angular fluxes at the reflective boundary for radial direction are preserved and used for next iteration. Because the GENESIS code uses cyclic ray tracing, no approximation is necessary to "connect" ray traces at the boundary. In 3D geometry, angular flux storage at radial boundary would be excessive, especially for a large and multigroup problem. The GENESIS code has an alternative option for boundary angular flux treatment, i.e., no angular flux at radial boundary is preserved and the boundary angular flux is recalculated on the fly using the angular flux iteration, in which only incoming angular flux is evaluated and no tally for scalar flux and neutron current is taken. The GENESIS code also adopts rigorous boundary treatment for the axial direction but does not preserve boundary angular flux at the top and bottom boundaries as this would require excessive memory storage. When the reflective boundary condition is applied to both of the top and bottom boundaries, incoming angular fluxes are always recalculated on the fly using iterations for axial direction.

3. Recent developments and verifications

3.1. Treatment of anisotropic scattering using the concept of SPn method

3.1.1. Theory

In conventional core analyses, anisotropic scattering has been taken into account through transport correction on the total cross section and the assumption of isotropic scattering [22]. However, use of transport correction would introduce considerable prediction error, especially in highly heterogeneous and/or high leakage cores. Thus, accurate consideration of anisotropic scattering is important for high fidelity neutronics simulations.

Treatment of anisotropic scattering has been established with expansion of the real spherical harmonics functions, as shown in Eqs. (14) and (15). In this approach, $(L+1)^2$ moments are necessary to represent the angular distribution of an anisotropic neutron source, where L is the order of anisotropic scattering.

$$S(\boldsymbol{r},\boldsymbol{\Omega}) = \frac{1}{4\pi}\sum_{l=0}(2l+1)\sum_{m=-l}^{l}\Sigma_{sl}(\boldsymbol{r})\phi_{l,m}(\boldsymbol{r})R_{l,m}(\boldsymbol{\Omega}), \tag{14}$$

$$\phi_{l,m}(\boldsymbol{r}) = \int \psi(\boldsymbol{r},\boldsymbol{\Omega})R_{l,m}(\boldsymbol{\Omega})d\boldsymbol{\Omega}, \tag{15}$$

where $R_{l,m}(\boldsymbol{\Omega})$ is the real spherical harmonics function of (l,m) order.

For example, when anisotropic scattering up to P3 component is taken into account, 16 flux moments are necessary for each flux region in each energy group. Because detailed spatial and energetic resolutions are required in precise neutronics simulation, the memory requirement for angular moments is significant, especially for a large geometry.

Recently, an explicit angular representation of neutron angular flux/neutron source was proposed for the SPn method [23,24]. A significant advantage of the SPn method is the smaller number of angular flux moments required for calculation. In the SPn method, $(L+1)$ moments are necessary, in which the number is much smaller than that required in rigorous treatment using the real spherical harmonics functions.

This concept is introduced in the treatment of anisotropic scattering to reduce computational burden. In addition to the conventional treatment using the spherical harmonics function, the present method is implemented in the GENESIS code. In this approach, the angular distribution of the neutron source is described by:

$$S(\boldsymbol{r},\boldsymbol{\Omega}) \approx \frac{1}{4\pi}\sum_{l=0}(2l+1)\Sigma_{sl}(\boldsymbol{r})\phi_l(\boldsymbol{r})P_l(\boldsymbol{\Omega}\cdot\boldsymbol{\Omega}_{\boldsymbol{J}}), \tag{16}$$

$$\phi_l(\boldsymbol{r}) = \int \psi(\boldsymbol{r},\boldsymbol{\Omega})P_l(\boldsymbol{\Omega}\cdot\boldsymbol{\Omega}_{\boldsymbol{J}})d\Omega, \tag{17}$$

where $P_l(\boldsymbol{\Omega}\cdot\boldsymbol{\Omega}_{\boldsymbol{J}})$, $\boldsymbol{\Omega}$, and $\boldsymbol{\Omega}_{\boldsymbol{J}}$ are the Legendre polynomials, neutron flight direction, and neutron current direction, respectively.

As a more physically intuitive interpretation, we can consider the picture shown in Fig. 2. In the concept of the SPn method, a "major axis" is considered and angular distribution is assumed to be azimuthally symmetric around the major axis. This is a physical picture of the "locally 1D" model, i.e., we see this angular distribution in a 1D slab geometry. It should be noted that in the original Chao's derivation, the major axis is assumed to be parallel to the gradient of higher-order moment, $\nabla\phi_l(\boldsymbol{r})/|\nabla\phi_l(\boldsymbol{r})|$. However, in order to reduce memory requirement and computation time, in the present implementation we assumed that the major axis is parallel to $\boldsymbol{J}(\boldsymbol{r})/|\boldsymbol{J}(\boldsymbol{r})|$.

In Eqs. (16) and (17), the value of the Legendre polynomial $P_l(\boldsymbol{\Omega}\cdot\boldsymbol{\Omega}_{\boldsymbol{J}})$ should be evaluated in each mesh because the neutron current direction depends on the spatial position. This would seem to require significant computation time. However, it is important to remember that Eq. (17) is used only to evaluate a mesh average angular flux, which is obtained after transport sweep for a particular angular direction. In this sense, the number of evaluations for $P_l(\boldsymbol{\Omega}\cdot\boldsymbol{\Omega}_{\boldsymbol{J}})$ is limited. Actually, the computation time is negligible in actual implementation of the GENESIS code.

The calculation procedures using the above concept can be summarized as follows:

(1) Perform transport sweeps for particular azimuthal and polar directions. Then, calculate region average angular flux through spatial numerical integration with ray traces.
(2) Neutron current direction is set from the result of previous transport sweep. Neutron current vector is calculated by the conventional real spherical harmonics function. Note that the initial guess of neutron current vector is set to be zero.
(3) Estimate inner product of the normalized neutron current vector $\boldsymbol{\Omega}_{\boldsymbol{J}}$ and neutron flight direction $\boldsymbol{\Omega}$ in current transport sweep $(\boldsymbol{\Omega}\cdot\boldsymbol{\Omega}_{\boldsymbol{J}})$.
(4) The angular flux moment $(l>1)$ is evaluated by:

$$\phi_l = \sum_m \omega_m \Psi_m P_l(\boldsymbol{\Omega}\cdot\boldsymbol{\Omega}_{\boldsymbol{J}}), \tag{18}$$

where ω_m is the quadrature weight, Ψ_m is region average angular flux, and m represents index of discretized angular direction.

(5) Scattering source is set by:

$$S_m = \frac{1}{4\pi}\begin{pmatrix} \Sigma_{s0}\phi_0 \\ +3\Sigma_{s1}\begin{pmatrix}\phi_{1,-1}R_{1,-1}(\boldsymbol{\Omega_m}) \\ +\phi_{1,0}R_{1,0}(\boldsymbol{\Omega_m}) \\ +\phi_{1,1}R_{1,1}(\boldsymbol{\Omega_m})\end{pmatrix} \\ +\sum_{l=2}(2l+1)\Sigma_{sl}\phi_l P_l(\boldsymbol{\Omega_m}\cdot\boldsymbol{\Omega}_{\boldsymbol{J}}) \end{pmatrix}. \tag{19}$$

It should be noted that explicit angular flux moments up to first order are evaluated in order to estimate the neutron current vector. Thus, these moments $(\phi_{1,-1}, \phi_{1,0}, \phi_{1,1})$ are explicitly used. Eqs. (16) and (17) are applied to anisotropic angular moments of $l>2$.

(6) Repeat steps (1) to (5) until convergence.

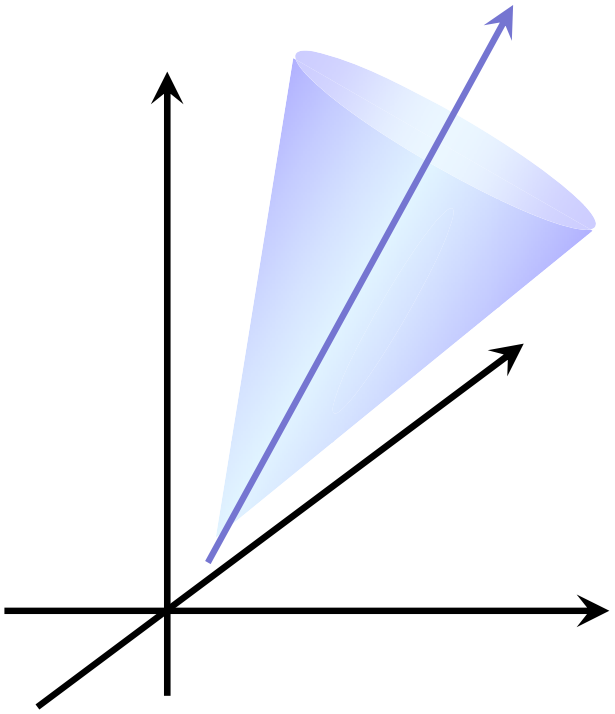

Fig. 2. Representation of angular distribution based on the concept of the SPn method. SPn, simplified Pn.

3.1.2. Numerical results

Accuracy of the treatment based on the concept of SPn method is verified through two problems.

The first one is the Lathrop forward scattering benchmark problem, which is a one-group fixed source problem [25]. Cross section and calculation geometry are shown in Fig. 3. Because the

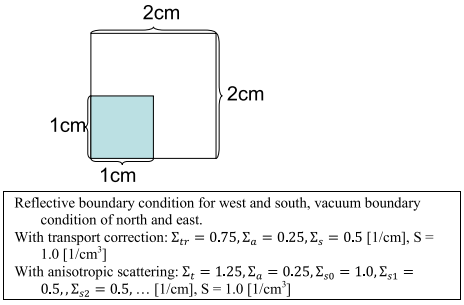

Fig. 3. Specification of the Lathrop forward scattering problem (2D case).

same magnitude of anisotropic scattering cross section is given in this benchmark problem, higher-order scattering calculation converges to that with the transport corrected cross section. In the original benchmark problem, the specification for the 2D problem is given, but in the present calculation, a 3D version is defined and used to confirm the accuracy of the present method in 3D geometry. As the angular distribution of flux is symmetric for upper and lower hemispheres of solid angle in 2D geometry, parts of angular moments expanded by the real spherical harmonics function are zero, which is not true for 3D geometry. The 3D version is constructed by a simple extension to the z direction, i.e., heights for neutron source and absorber regions are 1.0 cm and 2.0 cm, respectively, with reflective and vacuum boundary conditions for the bottom and top boundaries.

The following various treatments on anisotropic scattering are tested:

P0: No anisotropic component is taken into account.

P1, P2, P3: Up to P1, P2, P3 components are taken into account with expansion using the real spherical harmonics functions (the conventional and rigorous method).

SP2, SP3: Up to P2, P3 component is taken into account with expansion using the SPn concept (present method).

Note that the SP1 result is the same as the P1 result.

Calculation results are shown Figs. 4–7. The results with anisotropic scattering treatment through the real spherical harmonics function (rigorous approach) converged to the exact result, as expected. When the SPn approximation is applied for anisotropic source treatment, the results also approach the exact value but a slight bias is observed owing to approximation. The calculation results suggest that the present method can be used as an approximation to capture the higher order anisotropic scattering effect. It should be noted that, in the case of 1D slab geometry for the x, y, or z directions, the SPn treatment exactly reproduces the results obtained by rigorous anisotropic scattering treatment with the real spherical harmonics function. Convergence behavior of transport iteration with the SPn treatment is very similar to that of rigorous treatment with real spherical harmonics function.

The second problem is a typical pin cell and an array of 20 × 20 fuel pin cells surrounded by a thick water reflector, as shown in Fig. 8. Typical fuel rod type for PWR is assumed. The array of 20 × 20 fuel pins is an isolated fuel assembly in water. Leakage from the isolated fuel assembly is considered to be very large, and thus this configuration is appropriate to verify the accuracy of the present method. Two different fuel materials, i.e., 4.1 wt.% uranium dioxide (UO_2) and 12 wt.% Pu-total mixed oxide (Pu-t MOX) fuel, are used in the present test calculations because the effect of anisotropic scattering is especially large in MOX fuel. Anisotropic scattering up to P3 components is considered in 172 energy groups, and 2D calculations are carried out.

In addition to the treatment used in the previous test calculation, transport corrected cross section is also used in the second problem.

Tr: Isotropic scattering with transport correction. The extended transport approximation, which subtracts sum of out-scattering P1 components from the total cross section, is used. Self-scattering cross section is adjusted to preserve cross section balance.

Calculation results are shown in Table 1. Table 1 indicates that the anisotropic treatment based on the SPn concept shows reasonable accuracy. The results with the SPn method give better accuracy than that of the conventional P1 but worse than those of the conventional P2 or P3 cases, which uses explicit treatment of anisotropic scattering using the real spherical harmonics functions. As described previously, the SPn treatment exactly reproduces the reference (conventional) results obtained with real spherical harmonics functions in 1D slab geometry. In this context, when calculation geometry has a more “locally 1D” nature, the accuracy of the SPn treatment will increase, e.g., in a shielding calculation in a large geometry.

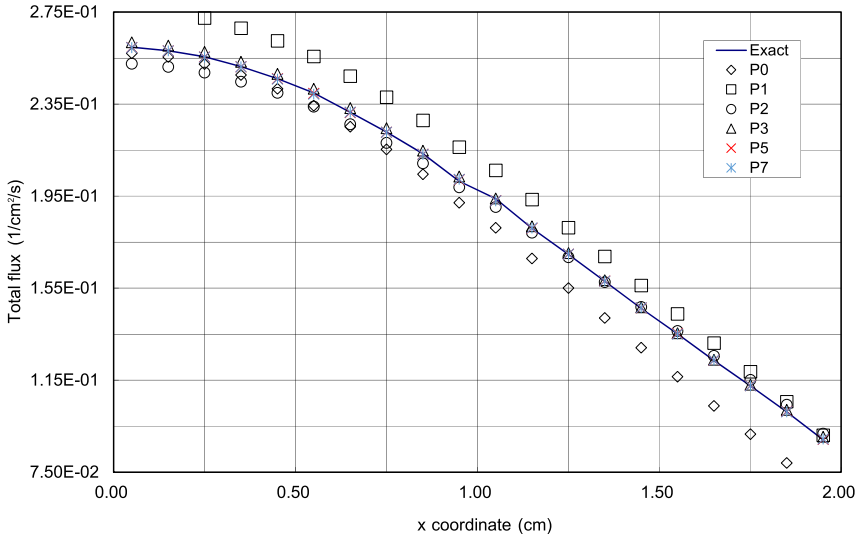

Fig. 4. Comparison of scalar flux distribution of the Lathrop forward scattering problem (rigorous treatment by real spherical harmonics, 2D case, y = 1.875 cm, the origin is southwest corner).

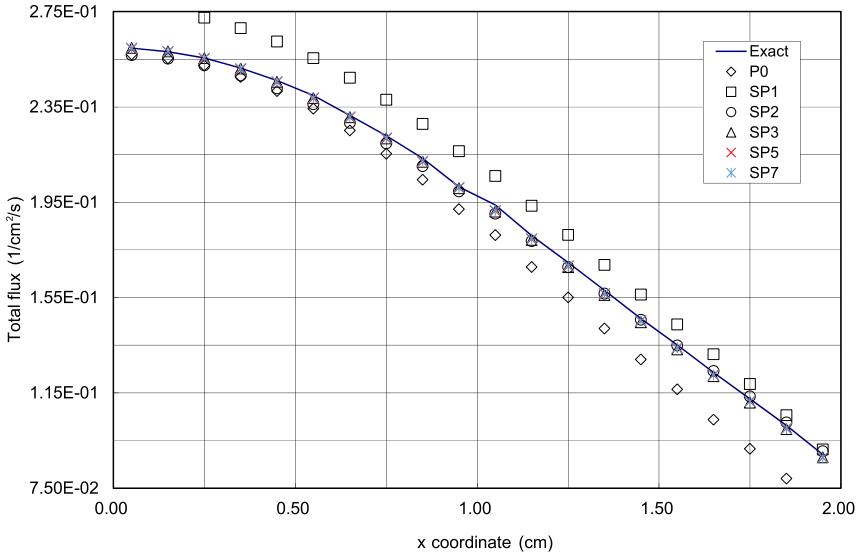

Fig. 5. Comparison of scalar flux distribution of the Lathrop forward scattering problem (SPn treatment, 2D case, $y = 1.875$ cm, the origin is southwest corner). SPn, simplified Pn.

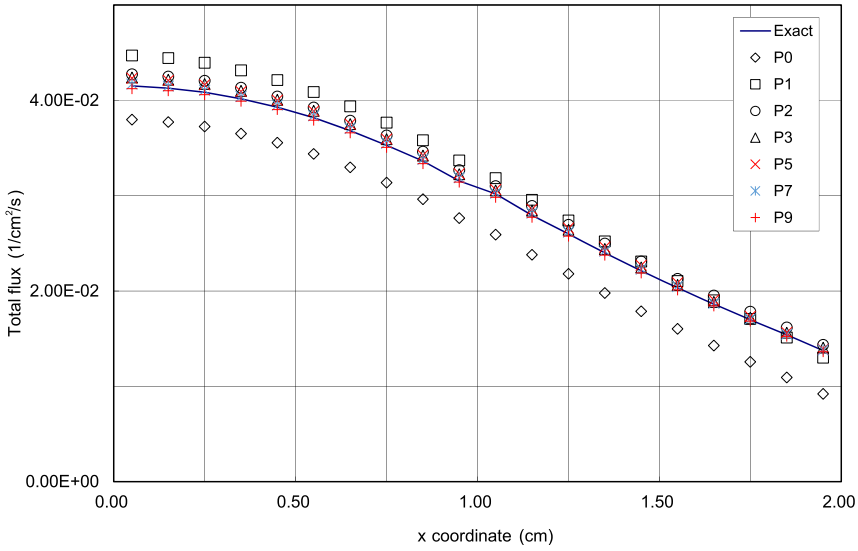

Fig. 6. Comparison of scalar flux distribution of the Lathrop forward scattering problem (rigorous treatment by real spherical harmonics, 3D case, $y = 1.875$ cm, $z = 1.95$ cm, the origin is southwest bottom corner).

In Table 1, the SPn results show slightly negative bias on *k*-effective and do not converge to the reference value as the order of SPn increases. It should be emphasized that the anisotropic treatment based on the SPn method is an approximation that does not necessarily converge to the rigorous value as the order of SPn increases because an assumption is made about the angular distribution of neutron flux. As described above, the accuracy of the present method depends on calculation conditions and geometry, and thus it should be considered an option for anisotropic treatment.

The present verification calculations suggest that the present approach on anisotropic scattering treatment will be a useful option for practical core analysis considering anisotropic scattering.

3.2. Stability and efficiency of GCMR/CMFD acceleration methods for highly voided condition

3.2.1. Outline

In the planar MOC method, axial planes are coupled through axial leakage between axial planes. It would be a cause of numerical instability under specific conditions, e.g., thin axial plane or large leakage for axial direction [26].

After the Fukushima-Daiichi accident, safety analysis for design extension conditions such as anticipated transient without scram has become required in Japan. Application of a precise core analysis method for such extreme conditions will be useful to quantify design margin in safety analyses. However, as described above, the planar MOC method would have difficulty analyzing highly voided conditions because axial leakage becomes extremely large. On the contrary, because the LEAF method does not use any approximation in the treatment of axial leakage, it would not incur instability in highly voided conditions.

For practical core analysis, use of an efficient acceleration method is indispensable. In the GENESIS code, the GCMR or CMFD acceleration methods can be used. The efficiency of these methods for typical core conditions has been established, but their applicability to highly voided conditions has not been confirmed.

In the present paper, efficiency and stability of the GCMR and CMFD methods used in the GENESIS code, coupled with various

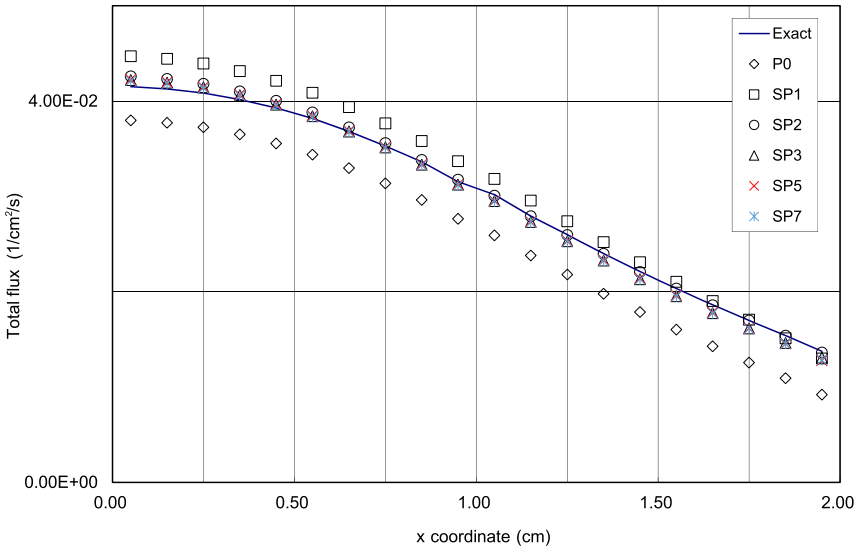

Fig. 7. Comparison of scalar flux distribution of the Lathrop forward scattering problem (SPn treatment, 3D case, $y = 1.875$ cm, $z = 1.95$ cm, the origin is southwest bottom corner). SPn, simplified Pn.

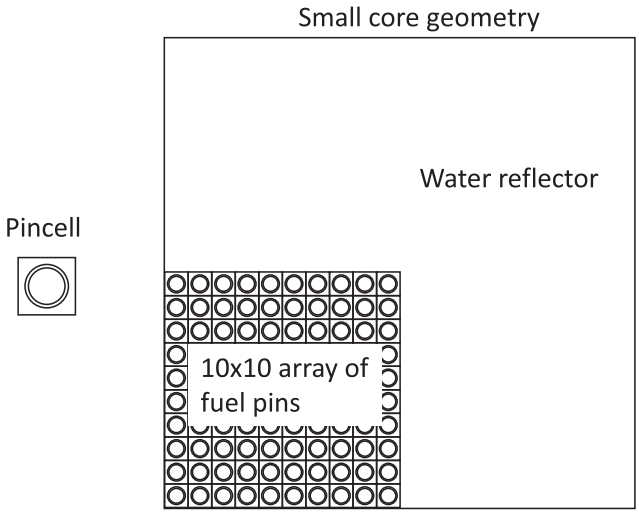

Fig. 8. Calculation geometry of UO_2/MOX pin cell and small core (all reflective boundary condition, 2D).

stabilization techniques, are investigated for highly voided conditions in LWR geometries.

3.2.2. Theory

The GCMR method is an acceleration method unifying the coarse mesh rebalance and the CMFD acceleration methods [18,19]. In the GCMR method, the following equation is used:

$$-\sum_{k\in S}\frac{\alpha^{-}_{i,k}\beta^{+}_{i,k}}{\alpha^{+}_{i,k}+\alpha^{-}_{i,k}}\phi_{j_k}S_k + \left(\sum_{k\in S}\frac{\alpha^{+}_{i,k}\beta^{-}_{i,k}}{\alpha^{+}_{i,k}+\alpha^{-}_{i,k}}S_k+\Sigma_{rem,i}V_i\right)\phi_i = Q_iV_i, \tag{20}$$

where

k surface index of a mesh

Table 1
Calculation results of k-effective with various treatments of anisotropic scattering.

Method	Pin cell		Small core	
	UO_2 4.1 wt.%	MOX 12 wt.% Pu-t	UO_2 4.1 wt.%	MOX 12 wt.% Pu-t
Tr	1.37576	1.19308	0.90434	0.85265
	0.05%	0.22%	−0.19%	−0.39%
P0	1.37531	1.19179	1.01768	0.93840
	0.02%	0.11%	12.23%	9.63%
P1	1.37461	1.18932	0.90222	0.85200
	−0.03%	−0.09%	−0.43%	−0.46%
P2	1.37513	1.19062	0.90639	0.85636
	0.01%	0.01%	0.03%	0.04%
P3	1.37501	1.19045	0.90607	0.85598
	—[a]	—	—	—
SP2	1.37476	1.18973	0.904968	0.85479
	−0.02%	−0.06%	−0.12%	−0.14%
SP3	1.37475	1.18969	0.90473	0.85446
	−0.02%	−0.06%	−0.15%	−0.18%

MOX, mixed oxide fuel; UO_2, uranium dioxide fuel.
[a] Reference value.

j_k neighbor mesh index through surface k
ϕ_{jk} average scalar flux of neighbor mesh adjacent to surface k
ϕ_i average scalar flux of region i
S_k area of surface k
$\alpha^{-}_{i,k}, \alpha^{+}_{i,k}$ acceleration factor at − and + surface of k
$\beta^{-}_{i,k}, \beta^{+}_{i,k}$, correction factor at − and + surface of k
Q_i neutron source of mesh i
V_i volume of mesh i
$\Sigma_{rem,i}$ removal cross section of mesh i

The correction factor in the GCMR method ($\beta^{-}_{i,k}, \beta^{+}_{i,k}$), are calculated by:

$$\beta^{-}_{i,k} = \frac{\left(J_{i\to j_k} - J_{j_k\to i}\right) + 2\alpha^{-}_{i,k}\left(J_{i\to j_k} + J_{j_k\to i}\right)}{\phi_i},$$
$$\beta^{+}_{i,k} = \frac{\left(J_{j_k\to i} - J_{i\to j_k}\right) + 2\alpha^{+}_{i,k}\left(J_{i\to j_k} + J_{j_k\to i}\right)}{\phi_i}, \tag{21}$$

where

$J_{i\to j_k}$ partial current from mesh i to j_k,
$J_{j_k\to i}$ partial current from mesh j_k to i
$\alpha^-_{i,k}$ acceleration factor at − side of surface k
$\alpha^+_{i,k}$ acceleration factor at + side of surface k

When $\alpha^-_{i,k}$ and $\alpha^+_{i,k}$ are set to be $D_i/\Delta x_{i,k}$, the GCMR method is equivalent to the one-node type CMFD method. Here, D_i and $\Delta x_{i,k}$ are diffusion coefficient and distance between center of mesh and surface k, respectively. By adjusting $\alpha^-_{i,k}$ and $\alpha^+_{i,k}$, the stability of the GCMR method can be controlled, as shown in the numerical results.

The CMFD acceleration method is a well-known and successful acceleration method applied to various iteration methods. The following balance equation is used in the CMFD method:

$$-\sum_{k\in S}\left(\widehat{D}_{i,k}+\tilde{D}_{i,k}\right)\phi_{j_k}S_k + \left(\sum_{k\in S}\left(\widehat{D}_{i,k}-\tilde{D}_{i,k}\right)S_k+\Sigma_{rem,i}V_i\right)\phi_i = Q_iV_i, \tag{22}$$

where

$$\widehat{D}_{i,k}=\frac{\alpha^+_{i,k}\alpha^-_{i,k}}{\alpha^+_{i,k}+\alpha^-_{i,k}},$$

$$\tilde{D}_{i,k}=-\frac{\left(J_{i\to j_k}-J_{j_k\to i}\right)+\widehat{D}_{i,k}\left(\phi_{j_k}-\phi_i\right)}{\phi_{j_k}+\phi_i},$$

$$\alpha^-_{i,k}=D_i/\Delta x_{i,k},$$

$$\alpha^+_{i,k}=D_{j_k}\Big/\Delta x_{j_k,k}.$$

Note that $\tilde{D}_{i,k}$ is generally called the current correction factor.

The CMFD and GCMR acceleration methods are very effective at reducing iterations of transport sweep. However, they show numerical instability when mesh size used in acceleration is optically large. In the GCMR method, numerical instability can be avoided by adjusting the acceleration parameters ($\alpha^-_{i,k}, \alpha^+_{i,k}$), but convergent efficiency is degraded.

In the LEAF method, spatial distribution inside a mesh is considered. The spatial distribution is expressed as a shape relative to mesh average scalar flux. When the CMFD and GCMR acceleration methods are applied, only mesh average scalar flux (flat distribution) is corrected with a rebalancing factor. Higher-order spatial moments are not directly accelerated.

In order to increase the convergence stability of the CMFD method, various methods have been investigated [26]. In the present study, the following stability techniques are used and tested.

(1) Effective diffusion coefficient

The normal diffusion coefficient ($1/3\Sigma_{tr}$) and the effective diffusion coefficient (Deff) [27], shown as Eq. (23), are used in this study.

$$D_i^{eff}=D_i\left(1+\Delta x_{i,k}\rho_{i,x}\Big/D_i\right), \tag{23}$$

where

$$\rho_{i,x}=\frac{\sum_{p=0}^{P}cos\theta_p\cdot w_p\cdot\alpha_{i,x,p}}{\sum_{p=0}^{P}w_p},$$

$$\alpha_{i,x,p}=\left(1+e^{-\gamma_{i,x,p}}\right)\Big/\left(1-e^{-\gamma_{i,x,p}}\right)-2\Big/\gamma_{i,x,p},$$

$$\gamma_{i,x,p}=\frac{2\Delta x_{i,k}}{3D_icos\theta_p},$$

where p is index of polar angle and θ_p is the angle from direction x.

(2) Damping factor

The damping factor [28] is applied to the correction factor of GCMR and to the current correction factor of CMFD, as shown in Eqs. (24) and (25), respectively:

$$\beta^{\ell+1}=w\beta^{\ell+1/2}+(1-w)\beta^{\ell}, \tag{24}$$

where

β^{ℓ}, $\beta^{\ell+1}$: correction factor used in the GCMR calculation after the lth and $(l+1)$th transport calculation
$\beta^{\ell+1/2}$: correction factor obtained from the $(l+1)$th transport calculation
w: damping factor

$$\tilde{D}^{\ell+1}=w\tilde{D}^{\ell+1/2}+(1-w)\tilde{D}^{\ell}, \tag{25}$$

where

$\tilde{D}^{\ell}$, $\tilde{D}^{\ell+1}$: current correction factor used in the CMFD calculation after the lth and $(l+1)$th transport calculation
$\tilde{D}^{\ell+1/2}$: current correction factor obtained from $(l+1)$th transport calculation

(3) Diffusion coefficient correction by additional constant

This method is called artificial grid diffusion (AGD) [26]. Eq. (26) is used for this correction in this study:

$$D'_i=D_i+a\cdot 2\Delta x_{i,k}, \tag{26}$$
a : constant specified by user

(4) Diffusion coefficient correction by multiplication constant

The improvement of convergence stability by the multiplication of constant to diffusion coefficient has been reported [19]. Eq. (27) is used for this correction in this study:

$$D'_i=b\cdot D_i, \tag{27}$$
b : constant specified by user.

(5) Number of inner iterations of MOC

The convergence becomes stable with increased number of inner iterations. One and two MOC inner iteration cases are investigated in this study.

3.2.3. Numerical results and discussions

The C5G7 2D and 3D benchmark problems are used for calculations [29]. In the original C5G7 2D/3D benchmark problems, UO_2–MOX color-set fuel assemblies are surrounded by water

reflector. In addition to the original benchmark problem, moderator inside two MOX fuel assemblies is voided to 99.9% in the present calculation. Calculation geometry is shown in Figs. 9 and 10.

Calculation conditions used in the GENESIS code are summarized as follows:

(2D case)

- Number of azimuthal angles: $48/2\pi$
- Number of polar angles: $8/\pi$ (Gauss Legendre)
- Track Spacing: 0.1 cm

(3D case)

- Number of azimuthal angles: $8/2\pi$
- Number of polar angles: $4/\pi$ (Gauss Legendre)
- Track spacing: 0.2 cm
- Acceleration mesh size for axial direction 3.0 cm

(2D and 3D cases)

- Convergence for *k*-effective: 5.0E−6
- Convergence for scalar flux: 1.0E−5
- Axial mesh size for 3D case: 3.0 cm

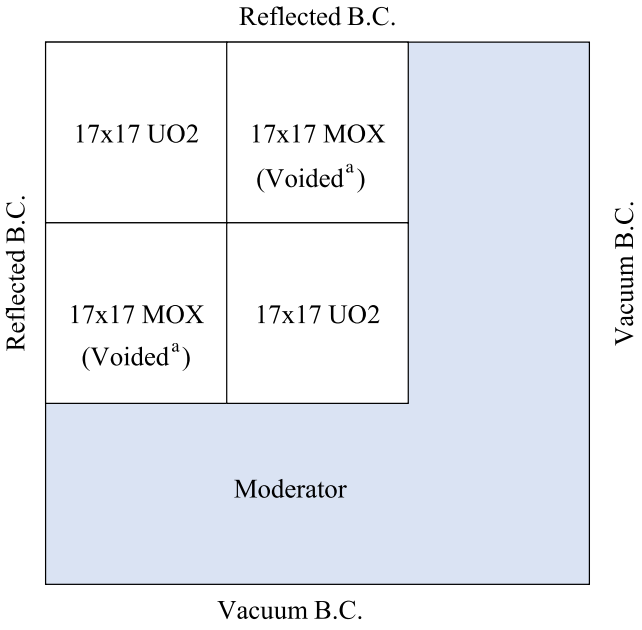

Fig. 9. Calculation geometry in this study. ([a] No void in the original C5G7 benchmark problem.). B.C., boundary condition; MOX, mixed oxide fuel; UO2, uranium dioxide fuel.

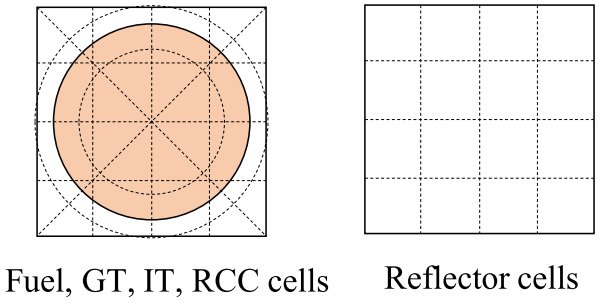

Fig. 10. Mesh divisions of each cell type. GT, guide thimble; IT, instrumentation thimble; RCC, rod cluster control.

- Acceleration mesh size for radial direction: 1 × 1/pin cell
- One or two transport sweep(s) (per inner transport iteration)

The above calculation conditions are not sufficient to obtain fully converged (accurate) results but are sufficient to verify the numerical stability of the acceleration methods. Note that prediction accuracy of the GENESIS code in these benchmark problems was confirmed through comparison with the Monte Carlo code [14].

The number of outer iterations required for convergence is shown in Figs. 11–14. In these figures, *w* indicates the damping factor in Eqs. (24) and (25), *a* and *b* indicate the parameters in Eqs. (26) and (27), respectively. The number of outer iterations is shown as zero for diverged cases.

From Figs. 11 and 12, the following observations are found for 2D calculation results:

- Numbers of outer iterations are similar both in the original (nonvoided) and the voided benchmark problems. The results indicate that the GCMR and CMFD acceleration methods can be directly applied to a highly voided condition in 2D geometry.
- By increasing number of inner iterations (from 1 iteration to 2 iterations), stability of acceleration calculation is increased.
- When no stabilization technique is applied ("None" in these figures), acceleration calculation shows divergence with one inner iteration. Thus, stabilization technique(s) are necessary to obtain converged results in this benchmark problem with an acceleration calculation.
- No significant difference from the viewpoint of efficiency is observed among stabilization techniques when appropriate acceleration parameters in these methods are chosen.
- The GCMR and CMFD methods show similar convergent behavior but GCMR shows a slightly more stable trend.

From Figs. 13 and 14, the following observations are obtained for 3D calculation results:

- In comparison to the 2D case, acceleration calculations tend to be unstable. If no stabilization technique (except for increasing number of inner iterations) is used, acceleration calculation diverges both for the original (nonvoided) and the voided cases.
- Application of the damping factor method for a correction factor, which is an effective approach in 2D geometry, is not very efficient in the present calculations. The present results seem to be inconsistent with the previous results in which the CMFD acceleration methods are applied to 3D transport calculation [26,30]. The difference between the previous and the present studies is the transport method used in the 3D calculation. In the previous study, the planar MOC method is used, in which axial planes are coupled through diffusion or low-order transport theory. By contrast, the GENESIS code uses the LEAF method, which explicitly treats angular flux propagation between axial planes. The LEAF method performs an explicit transport calculation not only for the radial direction but also for the axial direction. This difference has an impact on the stability of the acceleration method. It should be noted that the axial mesh size for the acceleration calculation is 3 cm, which is much larger than that for the radial direction (~1 cm). The GCMR and CMFD acceleration methods tend to become unstable for optically thick (large) meshes. The large mesh size for axial direction will also contribute to decreasing the stability of the acceleration in the GENESIS code.
- In contrast to the case of 2D geometry, numbers of iterations increase for voided condition. This trend is also caused by the nature of the LEAF method used in the GENESIS code.

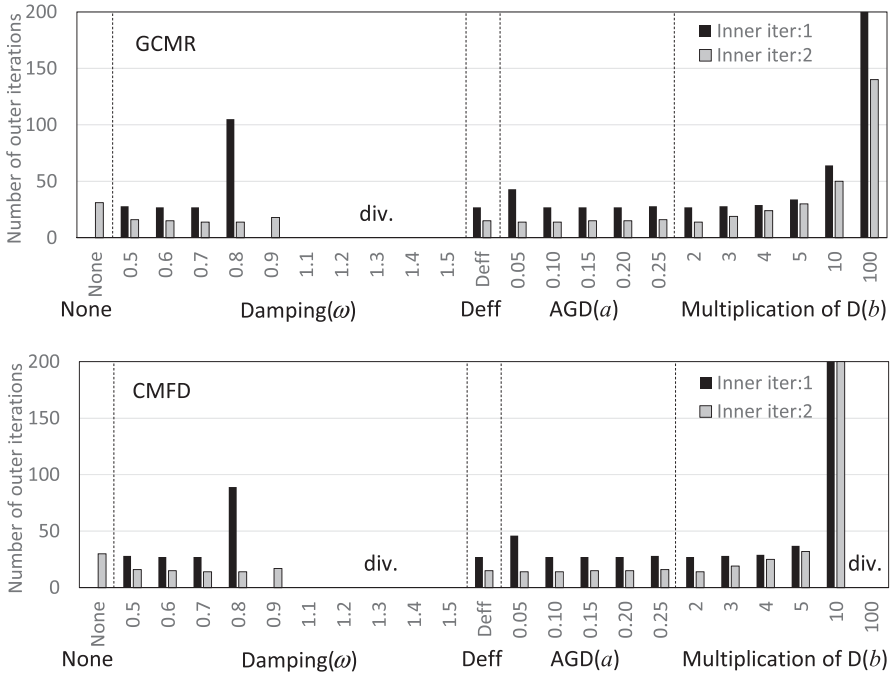

Fig. 11. Number of outer iterations (2D C5G7 original benchmark problem). AGD, artificial grid diffusion; CMFD, coarse mesh finite difference; D(b), diffusion coefficient given by Eq. (27); Deff, effective diffusion coefficient; div, divergence; GCMR, generalized coarse mesh rebalance.

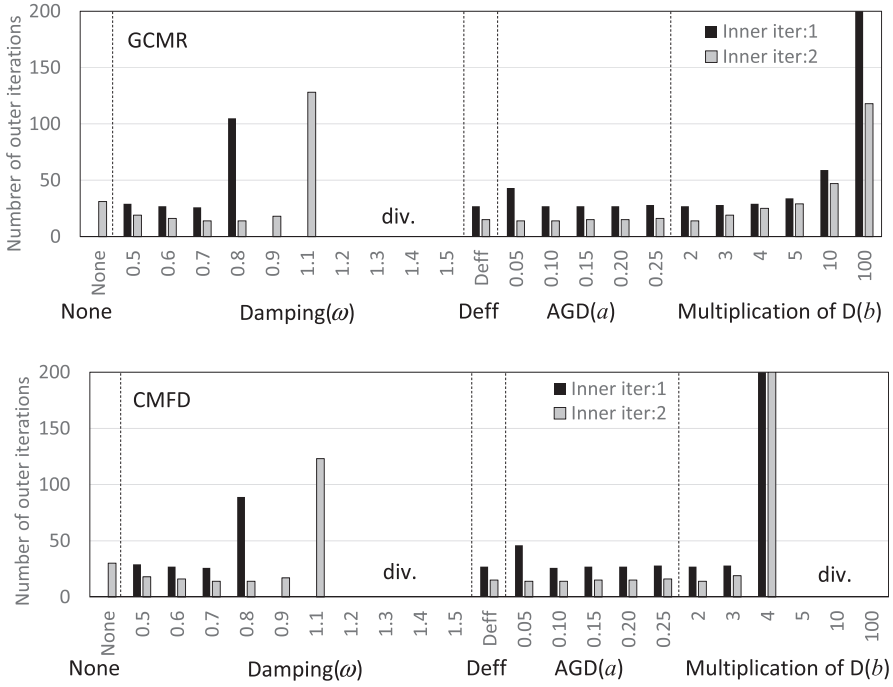

Fig. 12. Number of outer iterations (2D C5G7 voided benchmark problem). AGD, artificial grid diffusion; CMFD, coarse mesh finite difference; D(b), diffusion coefficient given by Eq. (27); Deff, effective diffusion coefficient; div, divergence; GCMR, generalized coarse mesh rebalance.

Considering Figs. 11–14, the following observation is obtained:

- Use of Deff and the AGD coefficient with $a = 0.25$ show stable convergence. Fig. 15 shows the ratio of the adjusted (corrected) diffusion coefficient to the unadjusted (original) diffusion coefficient. As shown in Fig. 15, Deff and AGD with $a = 0.25$ show similar trends for small ($h = 0.63$ cm) and large ($h = 10$ cm) mesh sizes. This is the root cause of the stable acceleration found when using these stabilization techniques.

As the computation time of the GCMR/CMFD acceleration is negligible, the relative computation time is proportional to the number of outer iterations.

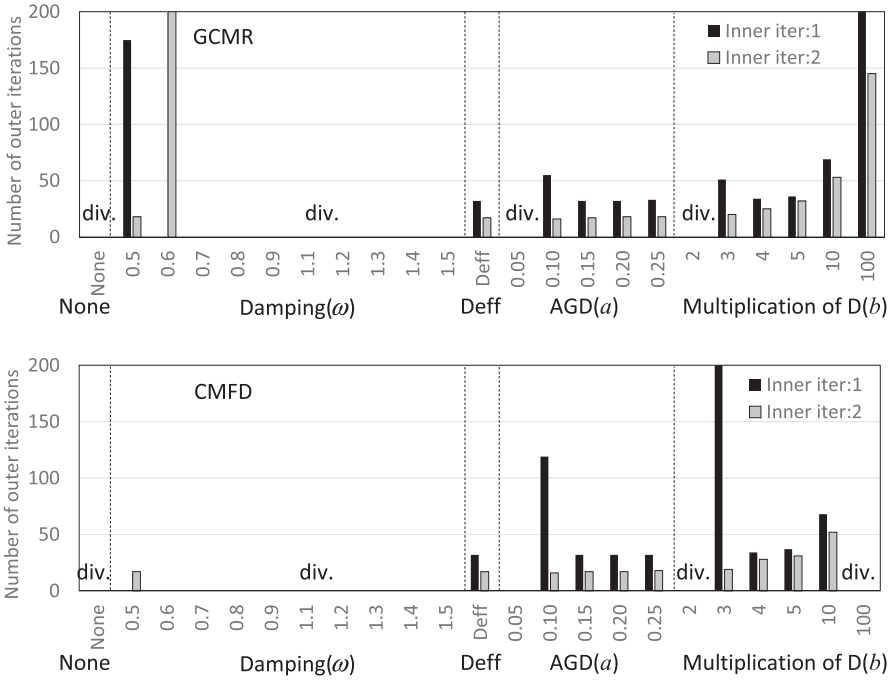

Fig. 13. Number of outer iterations (3D C5G7 original benchmark problem, unrodded). AGD, artificial grid diffusion; CMFD, coarse mesh finite difference; D(b), diffusion coefficient given by Eq. (27); Deff, effective diffusion coefficient; div, divergence; GCMR, generalized coarse mesh rebalance.

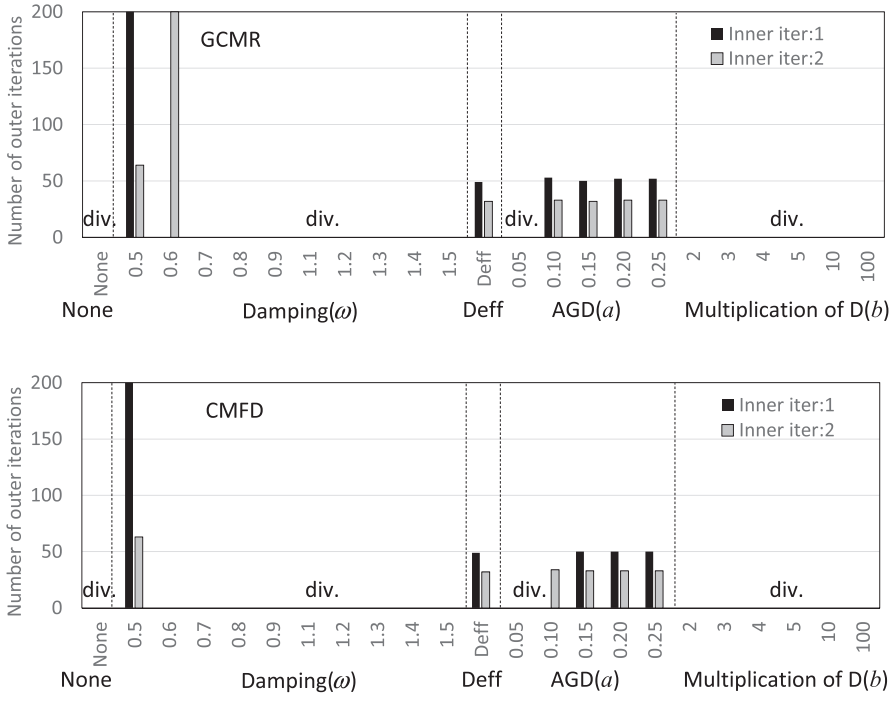

Fig. 14. Number of outer iterations (3D C5G7 voided benchmark problem, unrodded). AGD, artificial grid diffusion; CMFD, coarse mesh finite difference; D(b), diffusion coefficient given by Eq. (27); Deff, effective diffusion coefficient; div, divergence; GCMR, generalized coarse mesh rebalance.

In the LEAF method, higher-order spatial moments (i.e., linear and quadratic angular/scalar flux distributions) are considered in the transport calculation. In the GCMR and CMFD methods, however, the acceleration is carried out only for the average scalar flux and boundary angular fluxes, and relative shape of spatial distributions are not accelerated. Note that higher-order spatial moments of scalar flux in each region are expressed as the shape relative to the average scalar flux in a region. In principle, the relative shape of higher-order spatial moments will be accelerated by a low-order diffusion or transport calculation, but no attempt to do this is made in the GENESIS code. In our experience, the convergence of relative shapes of scalar flux and angular fluxes is

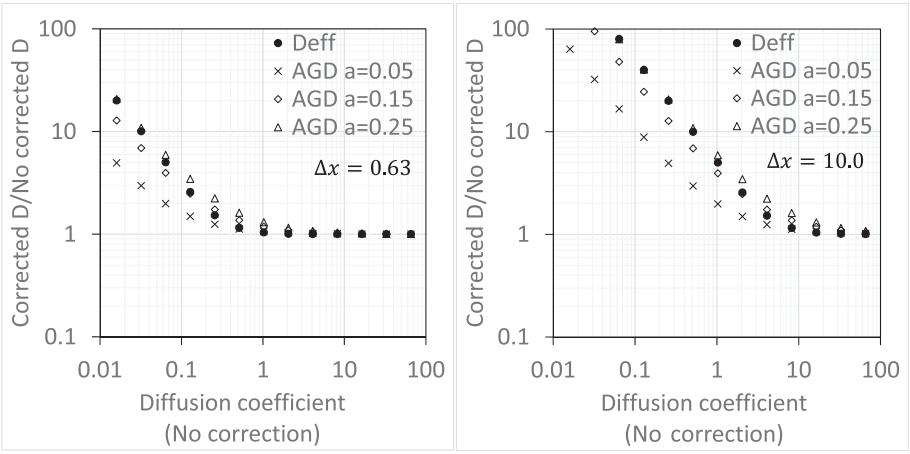

Fig. 15. Ratio of diffusion coefficients (corrected/not corrected) in effective diffusion coefficient (Deff) and artificial grid diffusion (AGD) coefficient for small ($\Delta x = 0.63$ cm) and large ($\Delta x = 10.0$ cm) mesh sizes. a, parameter used in Eq. (26); D, diffusion coefficient.

much faster than the magnitude of average scalar flux and angular fluxes, and thus the present treatment is justified. An acceleration calculation for higher-order spatial and angular moments would be an interesting topic but out of the scope of the present paper.

The present work is based on numerical results. Theoretical work on the convergence rate, which is performed for the conventional 2D MOC and the planar MOC method [26,30], would be desirable to confirm the generality of the results obtained in the present work.

Through the present benchmark calculations, the capability to treat the highly voided condition in the GENESIS code is confirmed, and calculation conditions to realize stable acceleration are clarified.

4. Summary

A 3D transport code for heterogeneous geometry using the LEAF method, GENESIS, is being developed at Nagoya University. In the present paper, the LEAF method and an overview of the GENESIS code are briefly reviewed. Then, to illustrate recent developments of the GENESIS code, application of the SPn concept for the treatment of anisotropic scattering and numerical stability of the CMFD/GCMR acceleration methods for highly voided conditions are discussed.

The SPn concept will be useful to reduce memory storage burden, especially for multigroup and large-scale problems, because the present method can significantly reduce the number of flux moments required for anisotropic scattering. The verification results show reasonable accuracy in comparison with the conventional treatment using real spherical harmonics.

Stability of the GENESIS code for highly voided condition is verified using a special version of the C5G7 benchmark problems containing fully voided assemblies. Iteration stability for 3D geometry is lower than that for 2D geometry, but stable convergence can be achieved using the Deff or the AGD coefficient in the CMFD/GCMR acceleration method.

Conflicts of interest

The authors have no conflicts of interest directly relevant to the content of this article.

Acknowledgments

This work was supported in part by JSPS KAKENHI, Grant-in-Aid for Scientific Research (C) (16K06956).

References

[1] R. Sanchez, Prospects in deterministic three-dimensional whole-core transport calculations, Nucl. Eng. Technol. 44 (2012) 113.
[2] J.Y. Cho, H.G. Joo, K.S. Kim, S.Q. Zee, M.H. Chang, Three-dimensional heterogeneous whole core transport calculation employing planar MOC solutions, Trans. Am. Nucl. Soc. 87 (2002) 234.
[3] S. Kosaka, T. Takeda, Verification of 3D heterogeneous core transport calculation utilizing non-linear iteration technique, J. Nucl. Sci. Technol. 41 (2004) 645–654.
[4] H.G. Joo, J.Y. Cho, K.S. Kim, C.C. Lee, S.Q. Zee, Methods and performance of a three-dimensional whole-core transport code DeCART, in: Proc. PHYSOR 2004, Apr. 25–29, 2004 (CD-ROM).
[5] B. Kochunas, B. Collins, D. Jabaay, T.J. Downar, W.R. Martin, Overview of development and design of MPACT: Michigan Parallel Characteristics Transport Code, in: Proc. M&C2013, Sun Valley, ID, May 5–9, 2013 (CD-ROM).
[6] Y.S. Jung, C.B. Shim, C.H. Lim, H.G. Joo, Practical numerical reactor employing direct whole core neutron transport and subchannel thermal/hydraulic solvers, Ann. Nucl. Energy 62 (2013) 357–374.
[7] M. Ryu, Y.S. Junga, H.H. Cho, H.G. Joo, Solution of the BEAVRS benchmark using the nTRACER direct whole core calculation code, J. Nucl. Sci. Technol. 52 (2015) 961–969.
[8] M. Hursin, Full Core, Heterogeneous, Time Dependent Neutron Transport Calculations with the 3D Code DeCart (Ph.D. thesis), UC Berkeley, 2010.
[9] J.B. Taylor, D. Knott, A.J. Baratta, A method of characteristics solution to the OECD/NEA 3D neutron transport benchmark problem, in: Proc. M&C + SNA 2007, Monterey, CA, 2007.
[10] Z. Liu, H. Wu, L. Cao, Q. Chen, Y. Li, A new three-dimensional method of characteristics for neutron transport calculation,, Ann. Nucl. Energy 38 (2011) 447.
[11] B. Kochunas, T.J. Downar, Z. Liu, Parallel 3-D method of characteristics in MPACT, in: Proc. M&C2013, Sun Valley, ID, May 5–9, 2013 (CD-ROM).
[12] A. Giho, K. Sakai, Y. Imamura, H. Sakurai, K. Miyawaki, Development of axially simplified method of characteristics in three-dimensional geometry, J. Nucl. Sci. Technol. 45 (2003) 985.
[13] Y. Kato, T. Endo, A. Yamamoto, Development of Legendre expansion of angular flux method for 3D MOC calculation, in: Proc. PHYSOR2014, JAEA—Conf 2014-003, Japan Atomic Energy Agency, 2014.
[14] A. Yamamoto, A. Giho, Y. Kato, T. Endo, GENESIS – a three-dimensional heterogeneous transport solver based on the Legendre polynomial expansion of angular flux method, Nucl. Sci. Eng. 186 (2017) 1–22.
[15] Z. Weiss, G. Ball, Ray-tracing in complicated geometries, Ann. Nucl. Energy 18 (1991) 483.
[16] T. Jevremovic, J. Vujic, K. Tsuda, ANEMONA—a neutron transport code for general geometry reactor assemblies based on the method of characteristics and R-function solid modeler, Ann. Nucl. Energy 28 (2001) 125.
[17] S. Kosaka, E. Saji, Transport theory calculation for a heterogeneous multi-assembly problem by characteristics method with direct neutron path linking technique, J. Nucl. Sci. Technol. 37 (2000) 1015.
[18] K. Smith, J.D. Rhodes, Full-core, 2-D, LWR core calculations with CASMO-4E, in: Proc. PHYSOR, Seoul, South Korea, 2002 (CD-ROM).
[19] A. Yamamoto, Generalized coarse-mesh Rebalance method for acceleration of neutron transport calculations, Nucl. Sci. Eng. 151 (2005) 274.
[20] A. Yamamoto, K. Kirimura, Y. Kamiyama, K. Yamaji, S. Kosaka, H. Matsumoto, Angular dependent transmission probability method for fast reactor core transport analysis, Trans. Am. Nucl. Soc. 112 (2015) 736.
[21] K.S. Smith, R. Ferrer, J.D. Rhodes, Linear source approximation in CASMO5, in: Proc. PHYSOR2012, Knoxville, TN, USA, April 15–20, 2012 (CD-ROM).
[22] Z. Liu, K. Smith, B. Forget, A cumulative migration method for computing

rigorous transport cross sections and diffusion coefficients for LWR lattices with Monte Carlo, in: Proc. PHYSOR2016, Sun Valley, ID, May 1–5, 2016 (USB drive).
[23] Y.A. Chao, A new SPN theory formulation with self-consistent physical assumptions on angular flux, Ann. Nucl. Energy 87 (2016) 137.
[24] Y.A. Chao, A. Yamamoto, The explicit representation for the angular flux solution in simplified PN (SPN) theory, in: Proc. PHYSOR2012, Knoxville, TN, Apr. 15–20, 2012 (CD-ROM).
[25] R. Roy, Anisotropic scattering for integral transport codes: Part 2. Cyclic tracking and its application to XY lattices, Ann. Nucl. Energy 18 (1991) 511.
[26] M. Jarrett, B. Kochunas, A. Zhu, T. Downar, Analysis of stabilization techniques for CMFD acceleration of neutron transport problems, Nucl. Sci. Eng. 184 (2016) 208.
[27] E. Larsen, Infinite medium solutions to the transport equation, S_n discretization schemes, and the diffusion approximation, in: Proceedings of the Joint International Topical Meeting on Mathematics and Computation and Supercomputing in Nuclear Applications, Salt Lake City, UT, USA, 2001.
[28] L. Li, A Low Order Acceleration Scheme for Solving the Neutron Transport Equation, Massachusetts Institute of Technology, Cambridge, MA, 2013.
[29] OECD/NEA, Benchmark on Deterministic Transport Calculations Without Spatial Homogenisation — MOX Fuel Assembly 3-D Extension Case, vol. 16, NEA/NSC/DOC(2005), 2005.
[30] S. Yuk, N.Z. Cho, Comparison of 1-D/1-D fusion method and 1-D/1-D hybrid method in two-dimensional neutron transport problems: convergence analysis and numerical results, Nucl. Sci. Eng. 184 (2016) 151.